Temperature-controlled synthesis of MOF-derived Ni_3S_2/C nanocomposites for high-performance supercapacitors

Xin Wang, Jian Luan,* Ying Yang, Wen-Long Duan,* Tian-Fang Cui, Wen-Ze Li*

College of Science, Shenyang University of Chemical Technology, Shenyang, 110142, P. R. China

E-mails: jluan@syuct.edu.cn (J. Luan); wlduan@syuct.edu.cn (W. L. Duan); wzli@syuct.edu.cn (W. Z. Li)

S1. Preparation of electrode materials

The nickel foam was cut into 1 cm × 1 cm pieces, sonicated in 1 M HCl for 5 min, rinsed with deionized water, sonicated in acetone solution for 5 min, rinsed with deionized water, sonicated in anhydrous ethanol solution for 5 min, rinsed three times with deionized water, and dried in a vacuum oven at 60 °C for 12 h.

The active ingredients listed above were combined with carbon black and polyvinylidene difluoride (PVDF) in an 8:1:1 mass ratio, then thoroughly ground, and N-methyl pyrrolidone (NMP) solution was added. The resultant slurry material was applied to the treated nickel foam, which was then placed in a vacuum drying oven and dried for 12 h at 60 °C. After drying, the electrode material was compressed at a pressure of 10 MPa.

S2. Preparation of asymmetric supercapacitors

The positive electrode material was chosen from the electrode materials developed before. The negative electrode materials were manufactured as follows: The activated carbon (AC):Super P (carbon black):PVDF = 7:2:1 (m:m:m) mixture was thoroughly milled before being added to the NMP solution, which was processed in the same manner that the positive electrode components were. The electrolyte was produced using 1 M KOH. The diaphragm consisted of polypropylene (PP).

S3. Characterization

The JSM-IT 800 field emission scanning electron microscopy (SEM) was used to investigate the surface morphology and structure of the generated materials, as well as to

collect energy dispersive X-ray (EDX) spectra and atomic percentages. Powder X-ray diffraction (PXRD) patterns were used to determine the composition and phases (Bruker D8 Advance). Elemental valence states of the materials were determined using X-ray photoelectron spectroscopy (XPS, Thermo Fisher Scientific, ESCALAB 250 Xi). FTIR spectroscopy (Varian 640-IR) was utilized to determine the organic functional groups of the materials. The thermal stability of the resulting material was assessed using a thermogravimetric analyzer (Netzsch 449c).

S4. Electrochemical testing

Cyclic voltammetry (CV) at various scan rates, constant current charge/discharge (GCD), and electrochemical impedance spectroscopy (EIS) studies were performed to get better understanding of electrode kinetics, capacitance properties, and storage capacity. In addition, electrochemical parameters such as specific capacitance, energy density and power density have been calculated. All of the tests described above were carried out in aqueous solutions of 1 M KOH electrolyte on an electrochemical workstation equipped with a typical three-electrode electrochemical cell. Carbon rods served as counter electrodes, standard calomel electrodes (SCE) as reference electrodes, and manufactured electrodes as working electrodes.

Table S1 Comparison of R_{ct} and R_s values for Ni-MOF-a@S6, Ni-MOF-a@S8 and Ni-MOF-a@S10.

Material	R_s (Ω)	R_{ct} (Ω)
Ni-MOF-a@S6	0.154	1.409
Ni-MOF-a@S8	0.015	1.346
Ni-MOF-a@S10	0.124	1.435

Table S2 The CV curve area of Ni-MOF-a@S10 at different scan rates.

Scan rate (mV/s)	Curve area (C)
200	0.026
100	0.019
50	0.014
20	0.010
10	0.008
5	0.007

Table S3 Comparison of R_{ct} and R_s values for Ni-MOF-a@S6, Ni-MOF-b@S8 and Ni-MOF-b@S10.

Material	R_s (Ω)	R_{ct} (Ω)
Ni-MOF-b@S6	1.171	0.025
Ni-MOF-b@S8	0.140	1.409
Ni-MOF-b@S10	0.136	1.466

Table S4 Material specific capacitance data (F/g).

Material	0.5 A/g	1 A/g	2 A/g	5 A/g	10 A/g	15 A/g	20 A/g
Ni-MOF-a@S6	374.40	214.67	127.56	47.78	31.11	23.33	13.33
Ni-MOF-a@S8	172.00	173.20	182.00	142.00	86.00	48.00	24.00
Ni-MOF-a@S10	496.67	260.89	144.00	92.20	20.00	16.67	13.33
Ni-MOF-b@S6	374.50	284.67	208.89	84.44	15.56	10.00	8.89
Ni-MOF-b@S8	230.00	182.22	119.11	84.44	60.00	46.67	35.56
Ni-MOF-b@S10	117.40	99.56	75.11	41.11	24.44	20.00	17.78

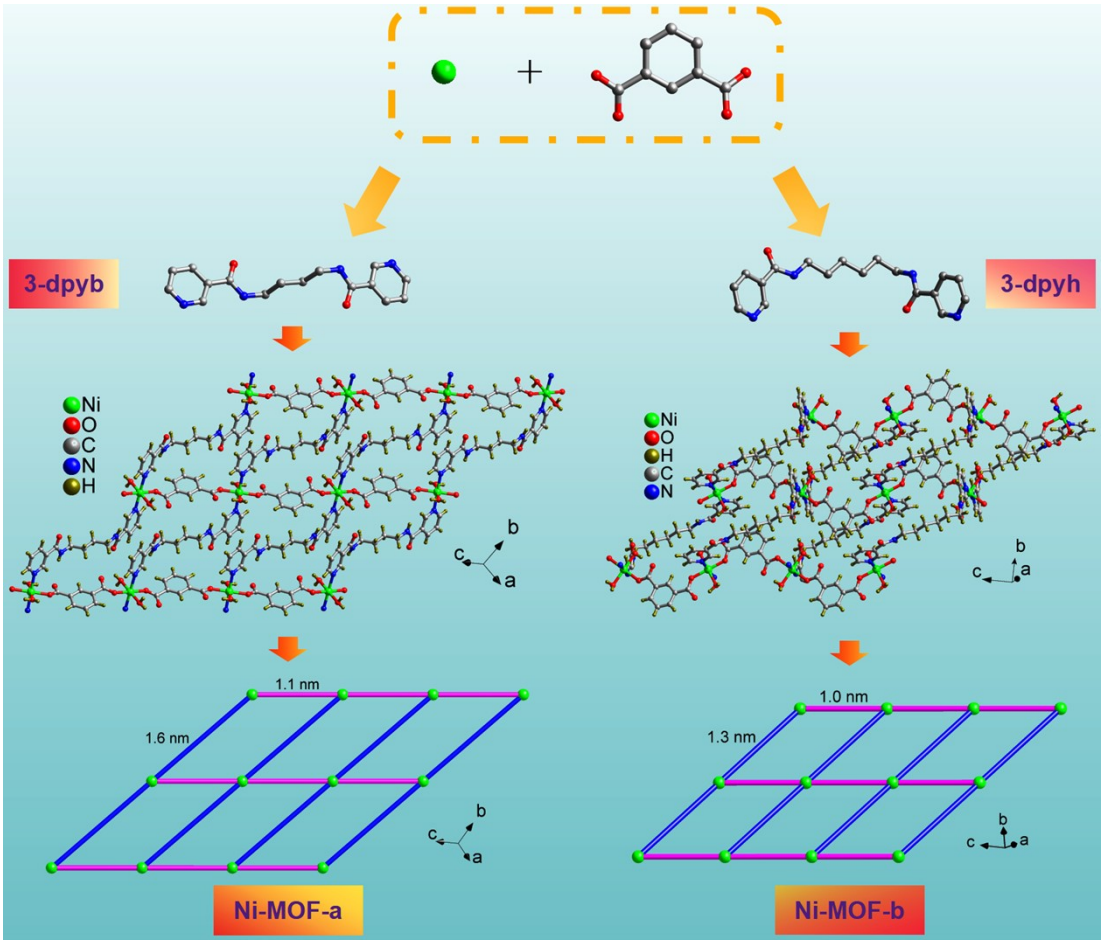

Fig. S1 Synthesis processes of Ni-MOFs.

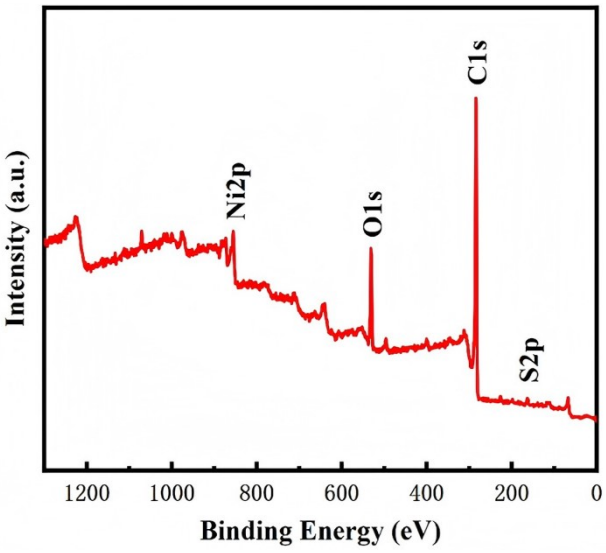

Fig. S2 The XPS spectrum of the as-prepared Ni-MOF-a@S10.

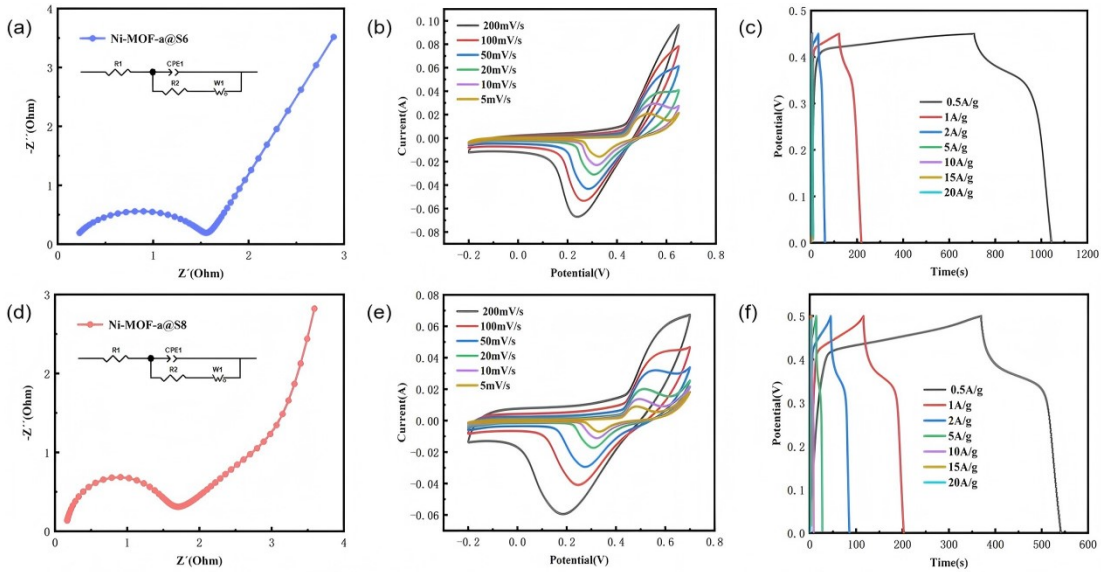

Fig. S3 EIS (a), CV (b) and (c) GCD cuvers of Ni-MOF-a@S6. EIS (d), CV (e) and (f) GCD cuvers of Ni-MOF-a@S8.

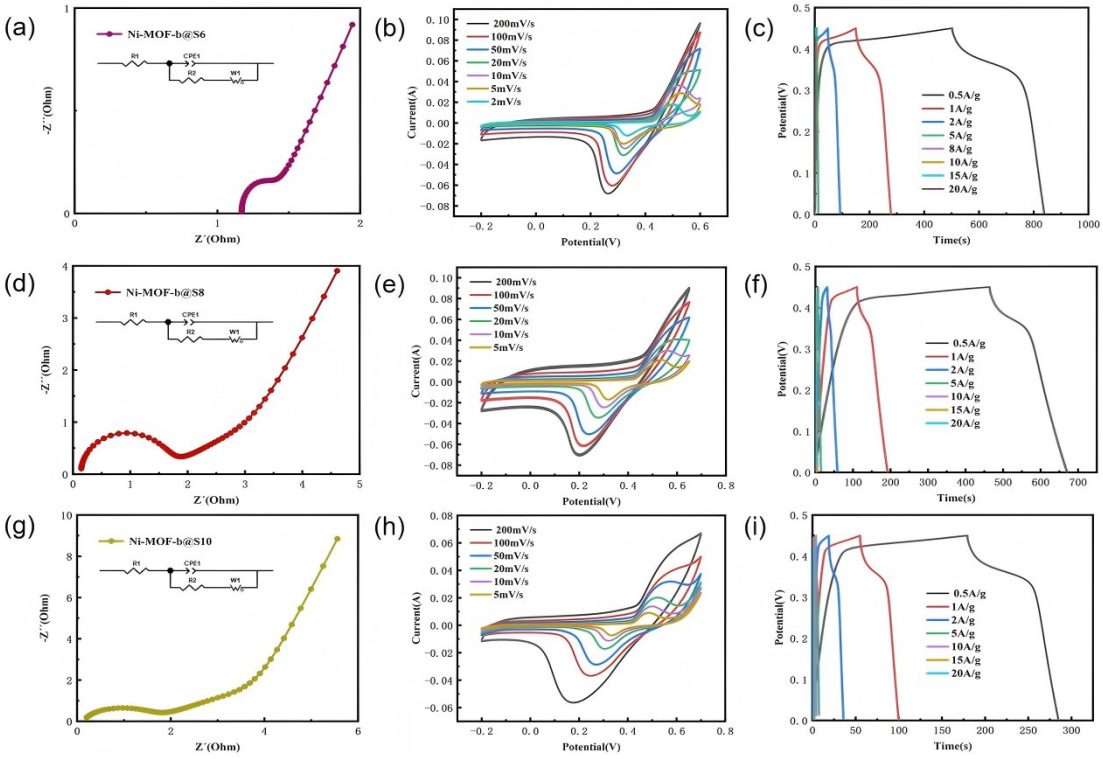

Fig. S4 EIS (a), CV (b) and (c) GCD cuvers of Ni-MOF-b@S6. EIS (d), CV (e) and (f) GCD curves of Ni-MOF-b@S8. EIS (g), CV (h) and (i) GCD cuvers of Ni-MOF-b@S10.

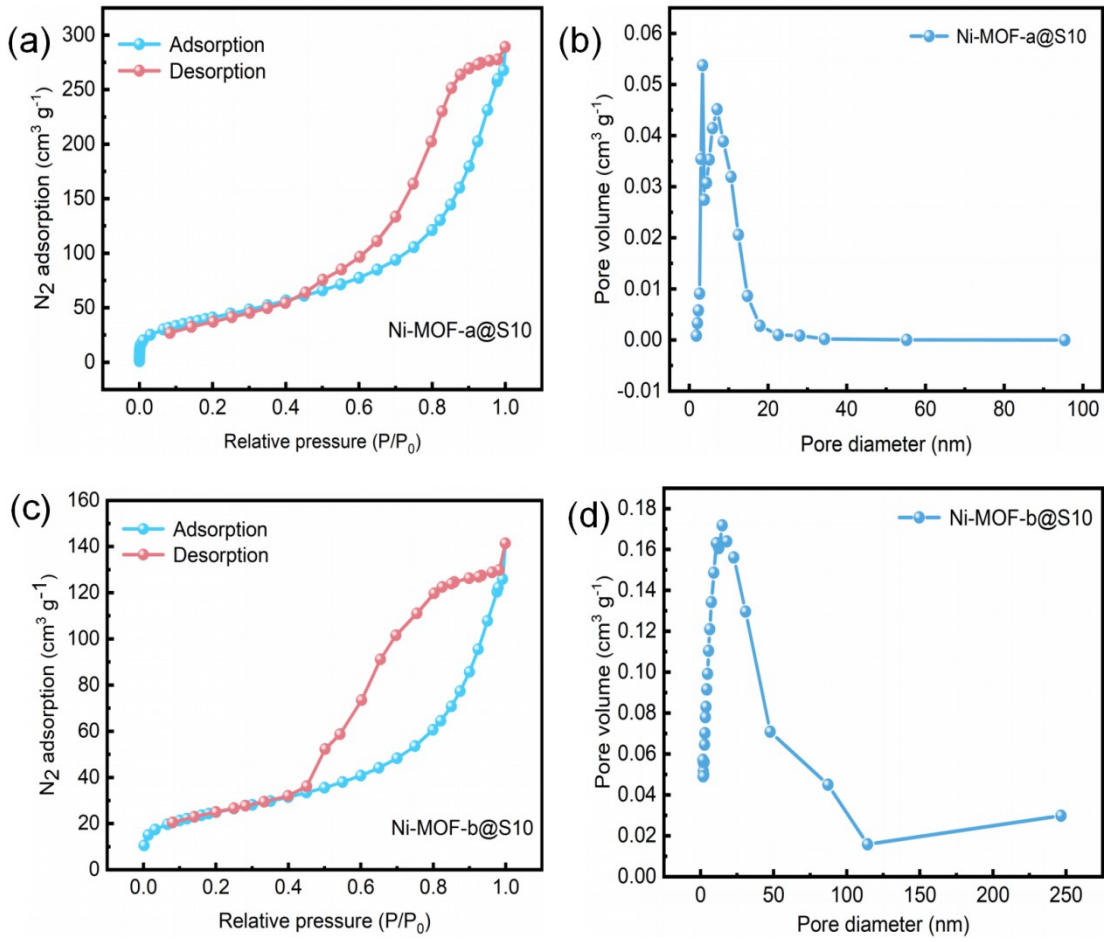

Fig. S5 Nitrogen adsorption and desorption isotherms of the Ni-MOF-a@S10 (a) and Ni-MOF-b@S10 (c). The pore size distributions of the Ni-MOF-a@S10 (b) and Ni-MOF-b@S10 (d).

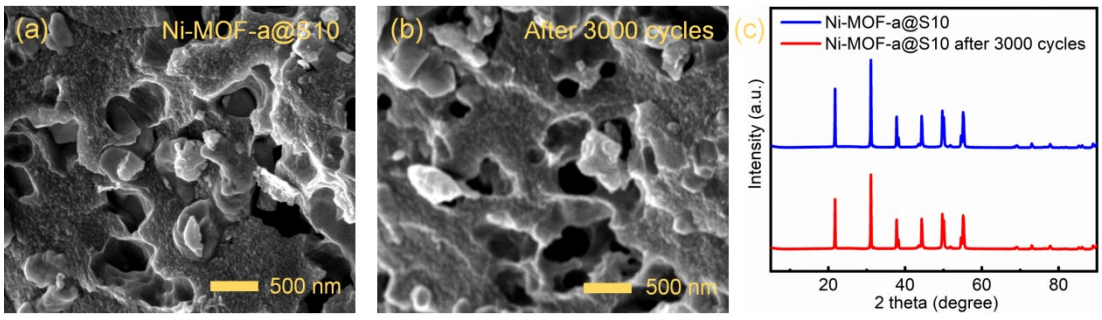

Fig. S6 SEM images of before (a) and after (b) 3000 cycles of Ni-MOF-a@S10. (c) PXRD patterns of before and after 3000 cycles of Ni-MOF-a@S10.

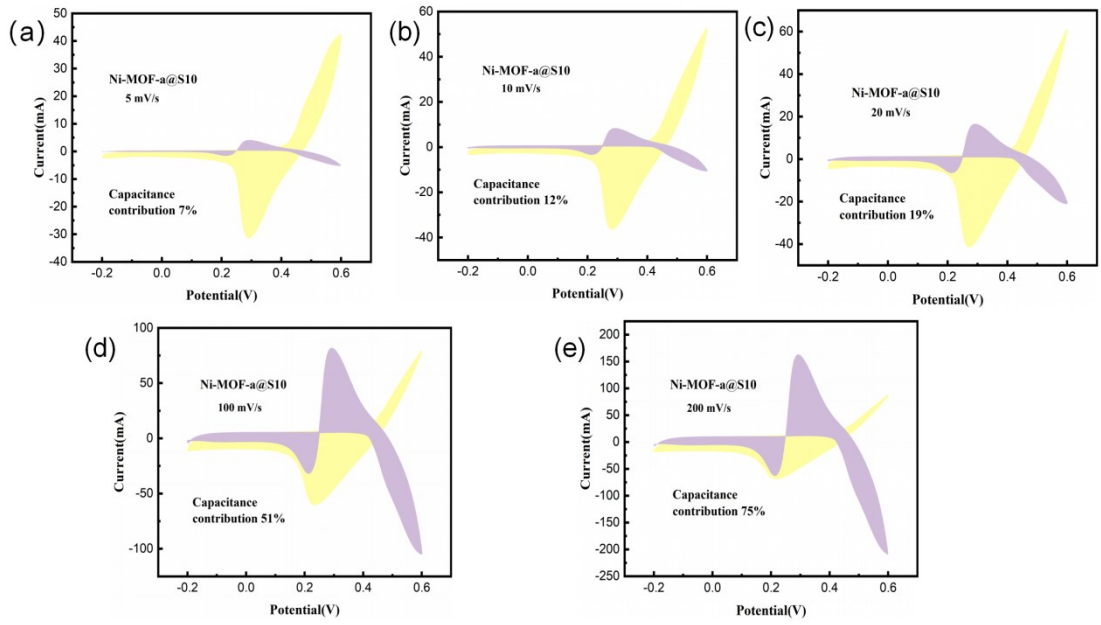

Fig. S7 Capacitive contribution of Ni-MOF-a@S10 at 5 mV/s (a), 10 mV/s (b), 20 mV/s (c), 100 mV/s (d) and 200 mV/s (e).

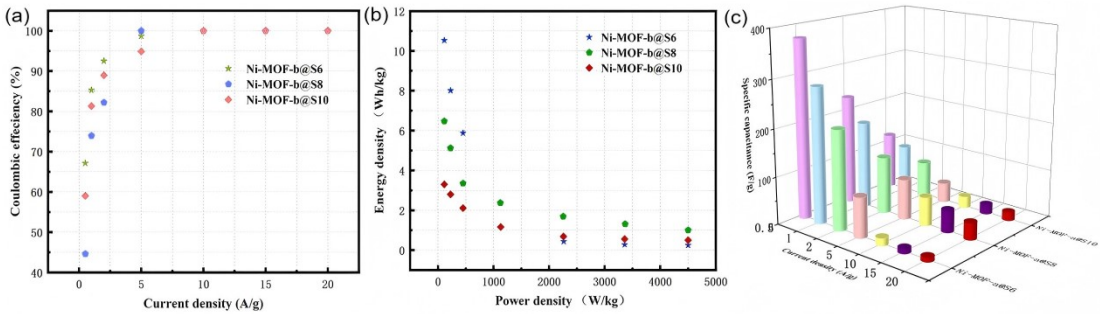

Fig. S8 Coulombic efficiency at various current densities (a), Ragone plots (b), and specific capacitance (c) for Ni-MOF-b@S6, Ni-MOF-b@S8 and Ni-MOF-b@S10.